

Hierarchical Auto-Regressive Model for Image Compression Incorporating Object Saliency and a Deep Perceptual Loss

Yash Patel^{2*}, Srikar Appalaraju¹, R. Manmatha¹
¹Amazon

²Center for Machine Perception, Czech Technical University, Prague, Czech Republic

patelyas@fel.cvut.cz, (srikara,manmatha)@amazon.com

Abstract

We propose a new end-to-end trainable model for lossy image compression which includes a number of novel components. This approach incorporates 1) a hierarchical auto-regressive model; 2) it also incorporates saliency in the images and focuses on reconstructing the salient regions better; 3) in addition, we empirically demonstrate that the popularly used evaluations metrics such as MS-SSIM and PSNR are inadequate for judging the performance of deep learned image compression techniques as they do not align well with human perceptual similarity. We, therefore propose an alternative metric, which is learned on perceptual similarity data specific to image compression.

Our experiments show that this new metric aligns significantly better with human judgements when compared to other hand-crafted or learned metrics. The proposed compression model not only generates images which are visually better but also gives superior performance for subsequent computer vision tasks such as object detection and segmentation when compared to other engineered or learned codecs.

1. Introduction

In the last two decades, the number of images captured and transmitted via the internet has grown exponentially [11]. This surge has increased both data storage and transmission requirements. Compression of images could be lossless [8, 37], that is, the original image can be perfectly reconstructed. A better compression rate may be obtained by using lossy methods such as JPEG [41], JPEG-2000 [37] and BPG [5]. The objective of these lossy methods is to obtain higher compression by removing the information which is least noticeable to humans. Note that these traditional codecs are hand-crafted and are not learned from the data.

There is also work on using learning to compress images.

While learned image compression from data using neural networks is not new [28, 17, 24], there has recently been a resurgence of deep learning based techniques for solving this problem [3, 4, 26, 32, 22, 29, 39]. These models are trained by jointly minimizing rate (storage or transmission requirement) and distortion (reconstruction quality), leading to a Rate-Distortion trade-off [35]. Our specific contributions are three-fold:

1. A novel hierarchical auto-regressive deep learned model with a feed-forward encoder-decoder is proposed for image compression. While auto-regressive models have been used before for compression, we believe this is the first hierarchical auto-regressive deep-learned model used for image compression.
2. An alternative learned perceptual metric, trained on compression specific artifacts is proposed. Since, this metric is a fully-convolutional-network (FCN), it is differentiable and is used for training.
3. The model accounts for salient regions in the images by: (a) allocating more bits to these regions and (b) giving higher weight to their reconstruction.

We now discuss the motivations and background for these contributions and describe the related work in this section.

Deep learning models for compression may be broadly categorized into three kinds of generative models: 1) Variational Auto-Encoders [19, 4, 3, 22], 2) Generative Adversarial Networks [32, 2] (GAN) [13] and 3) Auto-Regressive (AR) [40, 26]. While variational auto-encoders (VAEs) and auto-regressive models operate by estimating the probability density explicitly, GANs only have an implicit measure of density [13]. Although GANs are useful in very low bit-rate settings as they can learn to synthesize the images [2], their superiority over AR and VAE is unclear for higher bit-rates. One difference between VAE and AE is that the former approximates the density, whereas auto-regressive models such as Pixel-CNNs, Pixel-RNNs [40] have an ex-

*This work was done during YP's internship at Amazon

Higher MS-SSIM ←



Figure 1: An example from the Kodak dataset [12]. In order of MS-SSIM values: Mentzer *et al.* [26] > Ballé *et al.* [3] > BPG [5] > JPEG-2000 [37]. However, the order of performance based on 5 human evaluations is: BPG [5] > Mentzer *et al.* [26] > JPEG-2000 [37] > Ballé *et al.* [3]. Visually the foreground and text in BPG is clearly better in quality.

PLICIT and tractable measure of density either in the pixel space or in the quantized latent space.

In this paper, we propose a hierarchical auto-encoder (two-stage) with two 3D Pixel-CNN models which operate on quantized latent representations. During training, the 3D Pixel-CNNs give an explicit measure of the entropy of these quantized representation which via information theory directly relates to the bits required to store them after arithmetic coding [25]. While minimizing the estimated entropy leads to compression, the reconstructed image should be as close to the original as possible. Thus the estimated entropy is usually jointly minimized with a reconstruction loss such as mean-squared-error (MSE) or multi-scale structured similarity index (MS-SSIM) [43].

Lossy image compression models are compared by plotting the rate-distortion curve (rate in bits-per-pixel on the x-axis vs the distortion function on the y-axis). A common choice for the distortion function for compression models is MS-SSIM and PSNR [3, 4, 26, 22] both of which do not model the human perception well [30] (more in Sec. 2).¹ As deep learned codecs directly optimize on these evaluation metrics, it is natural for them to have high MS-SSIM or PSNR scores as compared to the engineered codecs such as JPEG-2000 [37], BPG [5] but the resulting decompressed images often look worse to a human (i.e. the actual distortion in the images is higher although the metrics report otherwise). Fig. 1 shows four different techniques ranked in descending order of MS-SSIM values. The 2nd and 3rd images have many more artifacts than the last two images (for example the text is not as clear in the first two approaches) which means that MS-SSIM is arguably not a good evaluation measure for compression.

The limitations of MS-SSIM and PSNR have been investigated in the past [44]. In fact, the super-resolution community has moved towards using a more sophisticated learned perceptual similarity metric [7, 6] for evaluation exactly for this reason. In spite of these short-comings, recent image

compression literature continues to evaluate models using MS-SSIM and PSNR [3, 4, 26, 22, 29, 32, 38, 39].

It has been observed that techniques trained on PSNR do well on PSNR evaluations but poorly when evaluated using MS-SSIM (and vice-versa) (see Lee *et al.* [22] but also see the two graphs on the right in Fig. where the ordering depends on the metric used and the training loss.) This makes it difficult to build practical compression systems. Here, we propose to use a deep learned perceptual similarity metric for evaluating and training image compression models. We also evaluate the compression techniques using human evaluation and show that the human evaluation results correlate well with the results of running object detector and image segmentation. That is, higher human evaluation scores tend to also lead to higher accuracies when running an object detector or image segmentation algorithm.

We start by evaluating the model proposed by Zhang *et al.* [44]. This model is trained on images with a number of different artifacts but the only compression artifacts are from JPEG compression. As Patel *et al.* [29] found, using the model has limitations for compression. We, therefore, create a compression specific perceptual similarity dataset. This dataset includes images generated from popular engineered [37, 41, 5] and learned compression methods [26, 3, 4, 29] and consists of 6 two alternative forced choices (2AFC) per comparison (Sec. 2).

While the JPEG [41] codec divides an image into uniform 8×8 blocks, BPG uses a hand-crafted metric to determine homogeneity and divides the more homogeneous regions into larger 64×64 blocks. This way, fewer bits are allocated to more homogeneous regions and more bits are allocated to complex/non-homogeneous image regions. BPG builds on the hypothesis that humans are more prone to notice artifacts in complex regions of the image. Using the motivation from BPG, and to the best of our knowledge unlike any other deep learning based compression method, we make use of object saliency maps for two purposes in our model: 1) **rate optimization**: more bits are allocated to

¹PSNR is directly related to MSE

the salient regions 2) **distortion optimization**: artifacts in salient regions are more heavily penalized.

The rest of the paper is structured as follows. In Sec. 2, the compression specific perceptual similarity dataset is presented and various metrics are compared against the human judgements. Sec. 3 describes our approach which is evaluated in Sec. 4. Sec. 5 concludes the paper.

2. Perceptual Similarity Metrics

In this section, we investigate various perceptual similarity metrics for both engineered and learned compression methods. We collect a compression specific perceptual similarity dataset and benchmark the existing hand-crafted metrics PSNR and MS-SSIM along with a learned metric LPIPS [44]. Following the recent evaluation setups in super-resolution literature [7, 6] we investigate various linear combinations of learned and hand-crafted perceptual similarity metrics as well.

2.1. Setup for Human Evaluations

The setup for collecting this dataset aligns with that of [44] and adapts two alternative forced choices (2AFC). Annotators are presented with two reconstructed versions of the same image from different compression methods along with the original image in the middle. They are asked to pick the image which is closer to the original image. Since at high bit rates the images may be similar to each other we provide the annotators with a synchronous magnifying glass and request them to scan the images as a whole in case of uncertainties. The setup was hosted on MTurk and on an average the evaluators spend 56 seconds on one sample.

The reconstructed images come from the following methods: Mentzer [26] *et al.*, Patel *et al.* [29], BPG [5] and JPEG-2000 [37]. 200 original images are used, comparisons are made at 4 different bit-rates and all possible combinations of methods are considered (6 for 4 methods). This results in 4,800 total samples for perceptual similarity studies. We use 3,840 samples for training and 960 held out samples for testing. For each such sample, we obtain 6 evaluations resulting in a total of 28,800 HITs.

2.2. Deep Perceptual Metric

The utility of using deep networks as a deep perceptual similarity metric has been well studied by Zhang *et al.* [44]. It has been observed that comparing internal activations from deep CNNs such as VGG-16 [36] or AlexNet [21] acts as a better perceptual similarity metric than MS-SSIM or PSNR. We follow Zhang’s approach and make use of activations from five *ReLU* layers after each *conv* block in the VGG-16 [36] architecture with batch normalization.

Feed-forward is performed on VGG-16 for both the original (x) and reconstructed image (\hat{x}). Let L be the set of

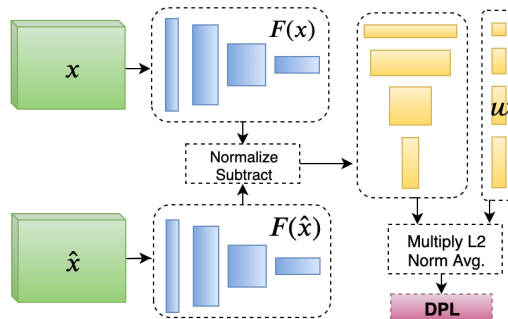


Figure 2: Deep Perceptual Loss: To compute perceptual similarity distance between the original x and reconstructed \hat{x} images - first compute the deep embeddings $F(x)$ and $F(\hat{x})$, normalize along the channel dimensions, scale each channel vector w (learned on perceptual similarity dataset), and take the ℓ_2 norm. Finally average across spatial dimensions and sum across channels.

layers used for loss calculation (five for our setup) and, a function $F(x)$ denoting feed-forward on an input image x . $F(x)$ and $F(\hat{x})$ return two stacks of feature activation’s for all L layers. The Deep perceptual loss is then computed as:

- $F(x)$ and $F(\hat{x})$ are unit-normalized in the channel dimension. Let us call these, $z_x^l, z_{\hat{x}}^l \in \mathbb{R}^{H_l \times W_l \times C_l}$ where $l \in L$. (H_l, W_l are the spatial dimensions).
- $z_x^l, z_{\hat{x}}^l$ are scaled channel wise by multiplying with the vector $w^l \in \mathbb{R}^{C_l}$
- The ℓ_2 distance is then computed and an average over spatial dimensions are taken. Finally, a channel-wise sum is taken, outputting the deep perceptual loss.

Eq.1 and Fig. 2 summarize the Deep perceptual loss computation. Note that the weights in F are learned for image classification on the ImageNet dataset [34] and are kept fixed. w are the linear weights learned on top of F on the perceptual similarity dataset using a ranking loss function [44]. In the next subsection, the *LPIPS* metric is referred to learning w on Berkeley-Adobe Perceptual Patch Similarity Dataset [44] and *LPIPS-Comp (Ours)* is referred to the setup when w is learned on the compression specific similarity data (Sec. 2.1). Note that *LPIPS-Comp* is used as the Deep perceptual loss (DPL).

$$DPL(x, \hat{x}) = \sum_l \frac{1}{H_l W_l} \sum_{h,w} \|w_l \odot (z_{\hat{x},h,w}^l - z_{x,h,w}^l)\|_2^2 \quad (1)$$

2.3. Analysing of Metrics for Image Compression

A comparison of various metrics is provided in Fig. 3. We start by computing the 2AFC score of a human evaluator. Then, we report the performance of two hand-crafted

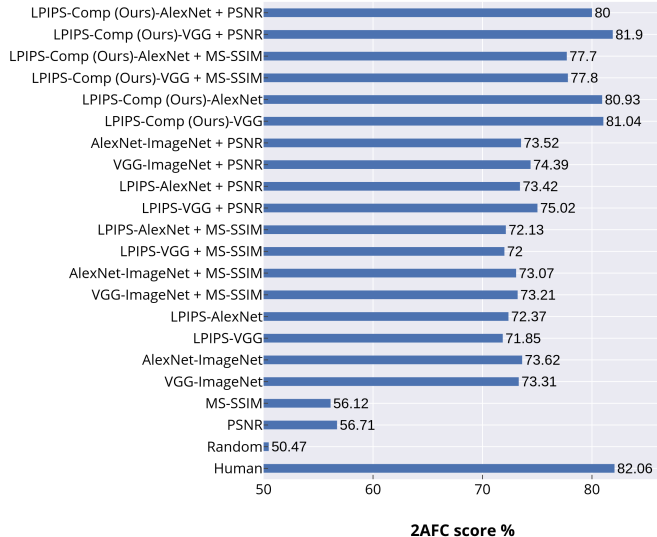


Figure 3: Comparison of various hand-crafted and learnt perceptual similarity metrics on the test set.

metrics PSNR and MS-SSIM. Note that these are the most popular metrics used in the compression literature to report the state-of-the-art [26, 22, 4, 3, 32, 27]. However, as shown in the figure the 2AFC scores for them (MS-SSIM and PSNR) are fairly low and thus they do not align well with the human perceptual similarity.

A naive similarity metric may be obtained by using AlexNet [21] or VGG-16 [36] trained on ImageNet. These features are known to act as a better similarity metric [44] compared to PSNR or MS-SSIM. The features may be adapted better for perceptual similarity by following the framework presented in Sec. 2.2, that is linearly re-weighting the channels by learning the weight vector on a perceptual similarity dataset. When these weights are learned on a generic dataset with a large collection of distortions (*LPIPS* in Figure 3) such as the Berkely-Adobe dataset [44], we observe that the performance is slightly worse compared to directly using the ImageNet model. This clearly indicates a domain gap and establishes that using the similarity data of a different nature can have adverse effects. When these weights are trained on compression specific data (*LPIPS-Comp Ours*) in 3), the learned metric aligns much better with the human judgements as can be clearly seen in Fig. 3.

Finally, similar to the recent super-resolution evaluation metrics [7, 6], we investigate the linear combination of hand-crafted metrics PSNR and MS-SSIM and a learned metric. Unlike [7, 6], we learn the weight given to each metric on the compression specific similarity dataset. We do so by solving a linear optimization problem and employing RANSAC. We refer to the supplementary material for a detained explanation on learning these weights. We ob-

serve that *LPIPS-Comp (Ours)* when combined with PSNR almost achieves close to human 2AFC score.

3. Proposed Method

The objective function of any lossy image compression technique may be defined by a rate-distortion trade-off:

$$\min_{\mathbf{x} \sim \chi} (\alpha Rate(\mathbf{x}) + \beta Distortion(\mathbf{x}, \hat{\mathbf{x}})) \quad (2)$$

where \mathbf{x} is the image to be compressed drawn from a collection of images χ , $\hat{\mathbf{x}}$ is the reconstructed image, $Rate(\mathbf{x})$ is the storage requirement for the image and $Distortion(\mathbf{x}, \hat{\mathbf{x}})$ is a measure of distortion between the original and the reconstructed images.

As shown in Fig. 4a, our method consists of two encoders, two decoders, two quantization stages and two auto-regressive models for entropy estimation, all of which are trained jointly and in an end-to-end fashion. The first encoder takes the image as input and outputs latent representation $\mathbf{y} = E_1(\mathbf{x}) : \mathbb{R}^{W \times H \times 3} \rightarrow \mathbb{R}^{\frac{W}{8} \times \frac{H}{8} \times C_1 + 1}$ (3.1). Note that the number of channels in the bottleneck, C_1 is one of the hyper-parameters to train the models to obtain different bits-per-pixel values. A pre-trained network outputs the object saliency for the input image $\mathbf{s} = S(\mathbf{x}) : \mathbb{R}^{W \times H \times 3} \rightarrow \mathbb{Z}_2^{\frac{W}{8} \times \frac{H}{8} \times 1}$ (Sec. 3.4). The latent representations are first masked by saliency driven priors $\mathbf{y}_m = m_1(\mathbf{y}, \mathbf{s})$ (Sec. 3.4) and then quantized $\tilde{\mathbf{y}} = Q_1(\mathbf{y}_m) : \mathbb{R} \rightarrow \{c_{(1,1)}, \dots, c_{(1,L)}\}$ (Sec. 3.2) and fed to stage-two. Within stage two, the second encoder outputs the latent representations $\mathbf{z} = E_2(\tilde{\mathbf{y}}) : \mathbb{R}^{\frac{W}{8} \times \frac{H}{8} \times C_1} \rightarrow \mathbb{R}^{\frac{W}{32} \times \frac{H}{32} \times C_2 + 1}$ which are also masked $\mathbf{z}_m = m_2(\mathbf{z})$ (independent of saliency) and quantized with different centers $\tilde{\mathbf{z}} = Q_2(\mathbf{z}_m) : \mathbb{R} \rightarrow \{c_{(2,1)}, \dots, c_{(2,L)}\}$.

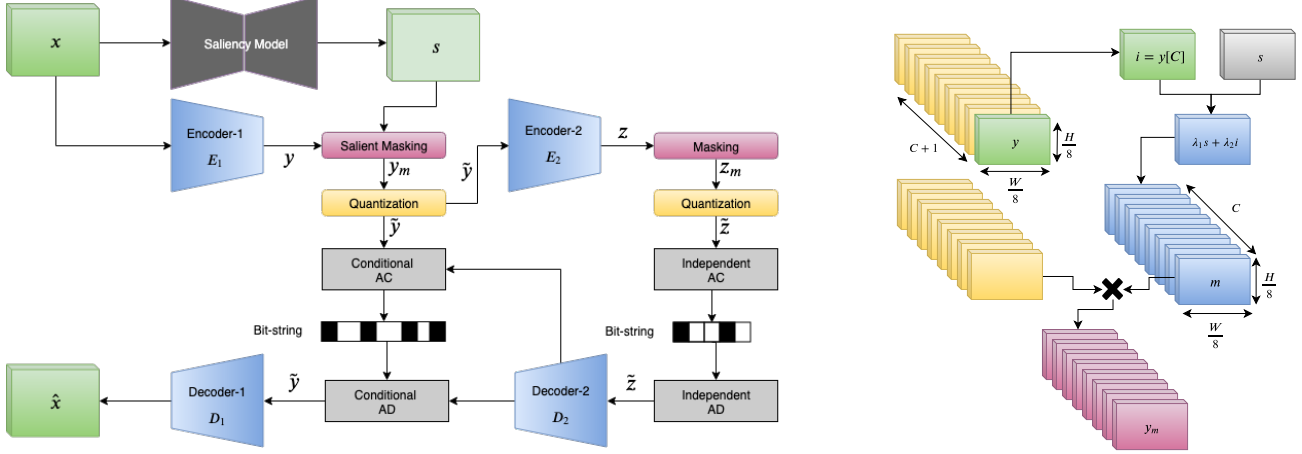
An auto-regressive image compression model operating on a quantized latent representation [26] factorizes the discrete representation using a basic chain rule [20]:

$$P(\tilde{\mathbf{y}}) = \prod_{i=1}^N p(\tilde{y}_i | \tilde{y}_{i-1}, \dots, \tilde{y}_1) \quad (3)$$

Our idea is to jointly learn an extra set of auxiliary representations $\tilde{\mathbf{z}}$ to factorize joint distribution using:

$$P(\tilde{\mathbf{y}}, \tilde{\mathbf{z}}) = P_{\Theta}(\tilde{\mathbf{y}} | \tilde{\mathbf{z}}) P_{\Phi}(\tilde{\mathbf{z}}) \quad (4)$$

Here Θ and Φ are the parameters of two 3D Pixel-CNN model where $P(\tilde{\mathbf{z}})$ is the second stage which is decoded first during the decompression stage. Thus for the first stage, quantized representations $\tilde{\mathbf{y}}$ are encoded and decoded by assuming that the $\tilde{\mathbf{z}}$ is available. In the subsequent sections, we describe each component in our proposed method.



(a) **Overall Method:** In the first stage, the input image is fed to the first encoder and the saliency model, the features are masked using an importance mask and the saliency mask. The masked features are then quantized and fed to the second-stage. Within the second stage the features are fed through another encoder, quantized and compressed independently in a lossless manner using adaptive arithmetic coding. A transformed version of these compressed representations is used to condition the compression (entropy estimation) of the first stage’s representation (standard adaptive arithmetic coding is used). Finally the compressed quantized representation are fed to the decoder to generate the reconstructed image.

(b) **Saliency Masking:** The last channel of the bottleneck $E_1(\mathbf{x})[C_1]$ from the first stage is used as an importance map \mathbf{i} . This importance map is linearly combined with the saliency mask \mathbf{s} and is expanded to match the dimensions of the bottleneck. Finally the bottleneck is masked using point-wise multiplication.

Figure 4: 4a provides an overview of our method while 4b illustrates the proposed saliency driven masking.

3.1. Encoder-Decoder

The method consists of two encoders and two decoders. The first encoder is a fifteen residual blocks [15] fully-convolutional network with three non-local/self-attention layers [42]. The first encoder involves down-sampling of the input image \mathbf{x} by a factor of 8. The second encoder takes the quantized representations from the first stage $\tilde{\mathbf{y}}$ as input, feed-forwards through five residual blocks [15], a non-local layer [42] and involves a further down-sampling by a factor of 4. $\tilde{\mathbf{z}}$ is $\frac{W}{32} \times \frac{H}{32}$ and fairly small compared to the input \mathbf{x} of $W \times H$. Thus, the number of bits required to store the second stage bit-string is very low (roughly 5% of the total storage). The decoders corresponding to these two encoders are mirror images.

The number of channels in the bottlenecks $\tilde{\mathbf{y}}$ or $\tilde{\mathbf{z}}$ is a hyper-parameter used to control the bits-per-pixel. In practice, we keep the number of channels the same for both of these bottlenecks. Both the bottlenecks have an extra channel for a hybrid of saliency mask and an importance map (Sec. 3.4 covers the details).

3.2. Quantization

Quantization is a non-differentiable function with gradients being either zero or infinite, thus any deep learnt model with quantization cannot be trained using backprop [33]. Thus, we adapt the soft vector quantization [1] in our model. More specifically, given a set of cluster centers

$C_1 = \{c_1, \dots, c_{L_1}\}$ the feed-forward is determined by:

$$\tilde{y}_i = Q_{C_1}(y) = \operatorname{argmin}_j \|y_i - c_j\| \quad (5)$$

during back-propagation, a soft cluster assignment is used:

$$\hat{y}_i = \frac{\exp(-\sigma \|y_i - c_j\|)}{\sum_{l=1}^{L_1} \exp(-\sigma \|y_i - c_l\|)} \quad (6)$$

Note that the quantization process is the same for both stages but with different sets of centers.

3.3. Hierarchical Auto-Regressive Model

First Stage: The representations of the first stage are encoded and decoded by conditioning on the second stage and may be fully factorized as:

$$P(\tilde{\mathbf{y}}|\tilde{\mathbf{z}}) = \prod_{i=1}^{i=N} P(y_i|y_{i-1}, \dots, y_1, D_2(\tilde{\mathbf{z}})) \quad (7)$$

The quantized representations of the first stage are lossless compressed using standard arithmetic coding where the conditional probabilities are estimated by a 3D pixel-CNN [20] which is conditioned on extra auxiliary representations $D_2(\tilde{\mathbf{z}})$. The 3D pixel-CNN is trained with cross-entropy minimization for a correct quantized center assignment:

$$P_{i,l}(\tilde{\mathbf{y}}) = p_{\Theta}(\tilde{y}_i = c_l|\tilde{y}_{i-1}, \dots, \tilde{y}_1, D_2(\tilde{\mathbf{z}})) \quad (8)$$

Thus the total entropy for the bottleneck is estimated using cross-entropy as:

$$CE = H_1(\tilde{\mathbf{y}}|\tilde{\mathbf{z}}) = \mathbb{E}_{\tilde{\mathbf{y}} \sim P(\tilde{\mathbf{y}}|\tilde{\mathbf{z}})} \left[\sum_{i=1}^{i=N} -\log(P_{i,l}(\tilde{y}_i)) \right] \quad (9)$$

Second Stage: The representations of the second stage are encoded independently and the distribution is factorized as a product of conditionals:

$$P(\tilde{\mathbf{z}}) = \prod_{i=1}^{i=M} P(\tilde{z}_i | \tilde{z}_{i-1}, \dots, \tilde{z}_1) \quad (10)$$

The second stage uses a separate 3D pixel-CNN [20], which is trained by minimizing:

$$CE = H_2(\tilde{\mathbf{z}}) = \mathbb{E}_{\tilde{\mathbf{z}} \sim P(\tilde{\mathbf{z}})} \left[\sum_{j=1}^{j=M} -\log(P_{j,l}(\tilde{z}_j)) \right] \quad (11)$$

Our objective with the second stage is to learn the auxiliary features which help in compressing the first stage representations more. Thus the gradients from Eq.9 are propagated to the second stage along with additional gradients from a reconstruction loss $mse(\tilde{\mathbf{y}}, D_2(\tilde{\mathbf{z}}))$.

Joint Optimization: The overall rate optimization $Rate(\mathbf{x})$ incorporates the masks from both stages, that is \mathbf{m}_1 and \mathbf{m}_2 as the weight to the cross-entropy computation for a given index in the bottleneck. The overall entropy is thus given by:

$$Rate(\mathbf{x}) = H = \mathbf{m}_1 H_1(\tilde{\mathbf{y}}|\tilde{\mathbf{z}}) + \mathbf{m}_2 H_2(\tilde{\mathbf{z}}) \quad (12)$$

3.4. Incorporating Object Saliency

The saliency mask \mathbf{s} such that $s_i \in \{0, 1\}$ is predicted by an off-the-shelf object saliency model [16], which was trained on MSRA10K data [9]. It is used in our compression model in two ways. Firstly, to mask quantized representations of the first stage, that is, more bits are allocated to the salient regions. Secondly, during the computation of distortion loss, to give higher weight to the reconstruction of the salient regions.

Salient Masking: The generated saliency mask is combined with an importance mask which helps in navigating the bit-rate convergence to a certain target value [26]. Similar to [26], the last channel of the bottleneck is treated as the importance mask $\mathbf{i} = E_1(\mathbf{x})[C_1]$. This importance mask is linearly combined with the saliency mask \mathbf{s} to make the compression driven by saliency. As illustrated in Fig. 4b, the final mask used is given by $\mathbf{m}_1 = \lambda_1 \mathbf{s} + \lambda_2 \mathbf{i}$. In practice we use $\lambda_1 = \lambda_2 = 1$, this way the model is able to incorporate saliency while at the same time is able to converge to a specified target bit-rate value.

This two-dimensional mask is expanded to match the dimensionality of the bottleneck as follows:

$$\mathbf{m}_1 : m_{i,j,k} = \begin{cases} 1 & \text{if } k < y_{i,j} \\ (y_{i,j} - k) & \text{if } k \leq y_{i,j} \leq k + 1 \\ 0 & \text{if } k + 1 > y_{i,j} \end{cases} \quad (13)$$

Finally, the bottleneck is masked by a pointwise multiplication with the binarization of \mathbf{m}_1 as $\mathbf{y}_m = \mathbf{y} \odot [\mathbf{m}_1]$.

Weighted Distortion Losses: Our hypothesis is that humans in general pay more attention to salient regions in the image. Thus, during training we give higher priority to the reconstruction of salient regions. This is achieved by decomposing the original and reconstructed images into salient and non-salient parts. Here distortion loss is computed on both separately and then linearly combined as:

$$w_1 D(\mathbf{x} \odot \mathbf{s}, \hat{\mathbf{x}} \odot \mathbf{s}) + w_2 D(\mathbf{x} \odot (\mathbf{1} - \mathbf{s}), \hat{\mathbf{x}} \odot (\mathbf{1} - \mathbf{s})) \quad (14)$$

$w_1 > w_2$, in practice, we set $w_1 = 0.75$ and $w_2 = 0.25$. Refer to the supplementary material for an illustration.

3.5. Model Optimization

The overall optimization is a rate-distortion trade-off (Eq. 2). The rate is determined by Eq. 12, the distortion is saliency driven and is governed by Eq. 14 where the distortion function D is a linear combination of the Deep perceptual loss DPL (Eq. 1) (LPIPS-Comp) and the mean-squared error between the original and the reconstructed images.

Training Details We make use of the Adam optimizer [18] with an initial learning rate of 4×10^{-3} and a batch-size of 30. The learning rate is decayed by a factor of 10 in every two epochs (step-decay). Further, similar to [26], we clip the rate term to $max(t, \beta R)$ to make the model converge to a certain bit-rate, t . The training is done on the training set of ImageNet dataset the from Large Scale Visual Recognition Challenge 2012 (ILSVRC2012) [34], with the mentioned setup, we observe convergence in six epochs.

By varying the model hyper-parameters such as the number of channels in the bottlenecks (that is C_1 and C_2), the weight for distortion loss (α), the target bit-rate (t), we obtain multiple models in the bit-per-pixel range of 0.15 to 1.0. Similarly we reproduce the models for [26, 3] at different BPP values. Note that in the case of [3] we used an MS-SSIM loss instead of MSE loss as was done in the original paper but this does not change the general conclusions of the paper. For Lee *et al.* [22], the authors provided us with the images on the Kodak dataset for human evaluations.

4. Results

Here we show the results of human evaluations on image compression. A different way to compare techniques is to see how the reconstructed images do on a computer vision task with a net pre-trained on uncompressed images

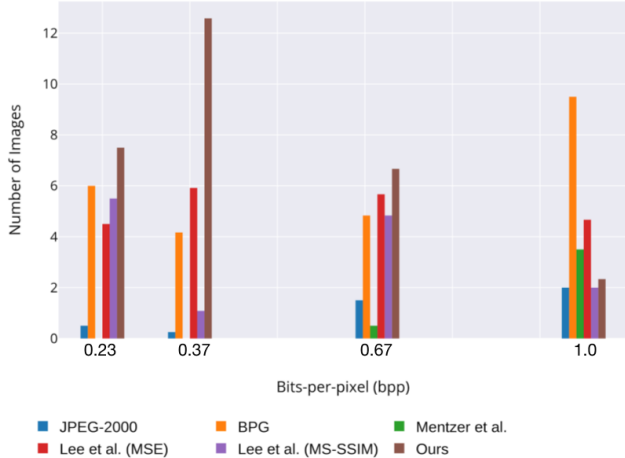


Figure 5: Human evaluations on the Kodak dataset. The y-axis shows the number of images for which a given method performs best. The x-axis shows the BPP values at which the comparisons were performed.

for that task. Specifically, we look at object detection and segmentation. Each lossy compression method creates certain kind of artifacts and these impact the task. For example Dwivedi *et al.* [10] show that for object detectors such as Faster-RCNN [31] region-based consistency is important and pixel level artifacts can affect the performance. Thus a compression method which distorts the region based consistency will perform poorly for object detection. This may be viewed as another kind of evaluation of a compression technique. We demonstrate that on all three metrics our approach does really well. Sec. 2 shows that the widely used metrics PSNR and MS-SSIM are inadequate for judging different compression methods. However, for completeness we also show results on PSNR and MS-SSIM.

Comparison and other Codecs: We compare the proposed method with the state-of-the-art image compression models from Lee *et al.* [22] based on variational autoencoders. We also compare to a single-level auto-regressive compression method Mentzer et al [26] and two engineered methods BPG [5] and JPEG-2000 [37]. We use the Kakadu² implementation for JPEG-2000 and use BPG in the 4:4:4 chroma format following [26, 32].

Quantitative Human Evaluations: We perform an extensive human evaluation study of five compression approaches across four different bits-per-pixel values (0.23, 0.37, 0.67, 1.0) on the Kodak dataset [12]. For the human evaluation, we follow the setup described in Sec. 2.1. The comparison is made in a pair-wise manner for all 15 possible combinations of the six methods (6C_2). For each such pair-wise comparison, we obtain five evaluations and determine the better performing method. Across different pair-

²<http://kakadusoftware.com/>

Method	0.23	0.37	0.67	1.0
JPEG-2000 [37]	23.2	29.1	34.4	36.8
BPG [5]	25.2	<u>32.5</u>	35.4	<u>37.7</u>
Mentzer <i>et al.</i> [26]	25.5	30.2	34.5	36.6
Lee <i>et al.</i> [22] (MSE)	<u>28.3</u>	-	<u>36.2</u>	37.6
Lee <i>et al.</i> [22] (MS-SSIM)	27.2	<u>32.5</u>	-	37.6
Ours (MSE + DPL)	29.3	33.7	36.6	37.9

Table 1: Object Detection on MS-COCO 2017 [23] validation set using Faster-RCNN [31]. The performance are reported using AP@[.5:.95]. , that is an average over different scales of IoU. Note that the performance on the original (uncompressed) images is 40.1%.

Method	0.23	0.37	0.67	1.0
JPEG-2000 [37]	20.2	25.4	30.1	<u>32.2</u>
BPG [5]	22.0	28.5	30.8	<u>32.2</u>
Mentzer <i>et al.</i> [26]	9.3	10.5	11.9	22.0
Lee <i>et al.</i> [22] (MSE)	<u>25.4</u>	-	<u>32.2</u>	33.2
Lee <i>et al.</i> [22] (MS-SSIM)	25.1	<u>28.9</u>	-	33.2
Ours (MSE + DPL)	26.1	30.0	32.3	33.2

Table 2: Instance segmentation on MS-COCO 2017 [23] validation set using Mask-RCNN [14]. The performance are reported using an average over multiple IoU values. Note that the performance on the original (uncompressed) images is 35.2%.

wise comparisons, the method which wins the most number of times performs best for the given image at a bit-rate. Thus, at each bit-rate we count the number of images for which a method performs best among the set of competing methods. Fig. 5 shows that our method is best according to the human evaluation across three bit-rate values (0.23, 0.37, 0.67). At a relatively higher BPP of 1.0 BPG outperforms all the other methods.

Qualitative Comparison: Please see Fig. 6 where we compare a Kodak dataset image (kodim15) with other methods. Note that our method better preserves the fine-grained details of the face than the other methods (see above the lip, paint patterns around the eye). For more such examples we refer the reader to the supplementary material.

Object Detection: We use a pre-trained Faster-RCNN [31] model with a *ResNet-101*[15] based backbone. With the original MS-COCO images, this model attains a performance of 40.1% AP . For each compression method, we compress and reconstruct the image at four different bit-rate values: 0.23, 0.37, 0.67, 1.0 (same values as used for human evaluation) and then we evaluate them for object detection. The performance of competing compression methods are reported in Tab. 1. It can be clearly seen that the proposed method outperforms the competing methods at bit-rates.

Instance segmentation: We make use of Mask-RCNN

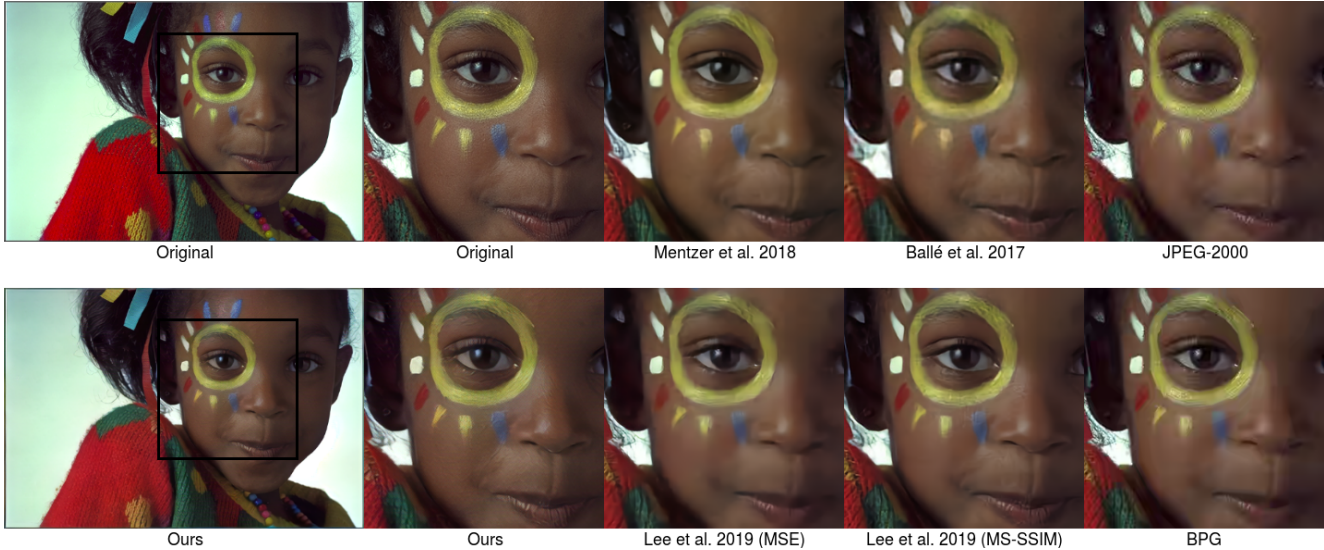


Figure 6: A qualitative example from the Kodak dataset [12] at **0.23 BPP**. Notice our method better captures the fine-grained details (lines above the lip, yellow circle around the eye) better than other approaches.

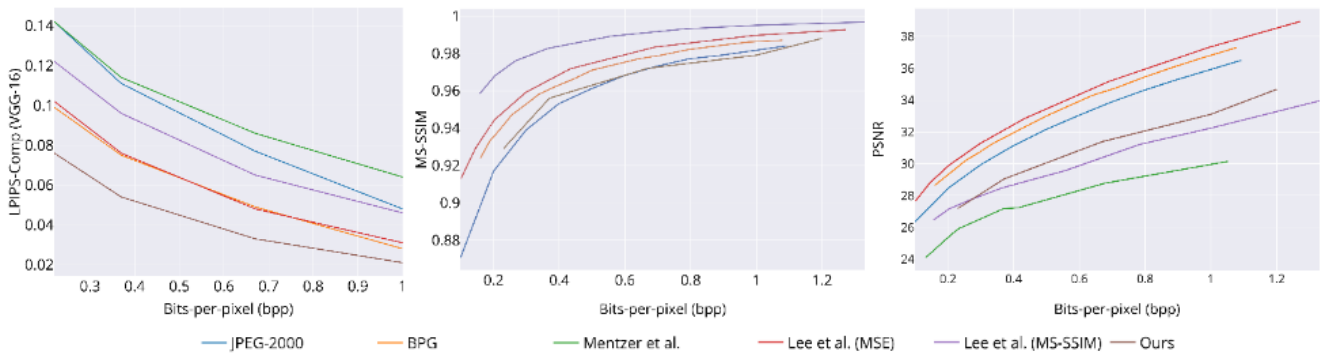


Figure 7: Different metrics on the Kodak dataset [12]. **Left:** (Perceptual Similarity) LPIPS-Comp (VGG-16) (Section 2.2) vs bits-per-pixel (BPP) (Lower is better). **Middle:** MS-SSIM vs bits-per-pixel (BPP). (Higher is better). **Right:** PSNR vs bits-per-pixel (BPP). (Higher is better). Best viewed in color.

[14] with a *ResNet-101* backbone for the task. The performance of different compression techniques is reported in Tab. 2. We observed that while Mentzer *et al.* [26] perform comparable to engineered methods on object detection, it performs far worse on Instance segmentation. It can be clearly seen from Tab. 2, that our method outperforms the competing methods at lower bit-rates while [22] performs identical at 1.0 BPP.

PSNR/MS-SSIM/LPIPS-Comp: For completeness we show the performance of these models on standard PSNR/MS-SSIM metrics in terms of Rate-Distortion curve. Please see Fig. 7 (right) for PSNR, Fig. 7 (middle) for MS-SSIM and Fig. 7 (left) for LPIPS-Comp (Sec. 2.2). We evaluate against two state-of-the-art learnt neural methods and two engineered codecs. We have a different model at each BPP (from 0.1 to 1.2). We used the images released by Mentzer and Lee et al. to plot the R-D curve.

These results corroborate our idea that evaluating on metrics PSNR/MS-SSIM does not align with human perceptual similarity. We can see that in spite of not doing well on these metrics, our method was the preferred method in the human study and also gave best performance on object detection and image segmentation tasks. Furthermore, the performance on PSNR or MS-SSIM is dependent on the distortion loss used during the training [22, 4], for our method the models are trained with a combination of MSE and DPL (LPIPS-Comp) as the distortion loss. Thus no particular attention has been paid to maximizing the performance on PSNR or MS-SSIM.

5. Conclusions

We described an approach to training and evaluating a deep image compression model using a deep perceptual

metric. It uses a hierarchical auto-regressive framework and takes object saliency into account. On human evaluations the model does better than the state-of-the-art on low bit rates. Images decompressed using the model also provide the best object detector and image segmentation results as compared to other image compression schemes.

Acknowledgment

We would like to thank Joel Chan and Peter Hallinan for helping us in setting up the human evaluations.

References

- [1] E. Agustsson, F. Mentzer, M. Tschannen, L. Cavigelli, R. Timofte, L. Benini, and L. V. Gool. Soft-to-hard vector quantization for end-to-end learning compressible representations. In *Advances in Neural Information Processing Systems*, pages 1141–1151, 2017.
- [2] E. Agustsson, M. Tschannen, F. Mentzer, R. Timofte, and L. Van Gool. Generative adversarial networks for extreme learned image compression. *arXiv preprint arXiv:1804.02958*, 2018.
- [3] J. Ballé, V. Laparra, and E. P. Simoncelli. End-to-end optimized image compression. *arXiv preprint arXiv:1611.01704*, 2016.
- [4] J. Ballé, D. Minnen, S. Singh, S. J. Hwang, and N. Johnston. Variational image compression with a scale hyperprior. *arXiv preprint arXiv:1802.01436*, 2018.
- [5] F. Bellard. Bpg image format, 2014.
- [6] Y. Blau, R. Mechrez, R. Timofte, T. Michaeli, and L. Zelnik-Manor. The 2018 pirm challenge on perceptual image super-resolution. In *Proceedings of the European Conference on Computer Vision (ECCV)*, pages 0–0, 2018.
- [7] Y. Blau and T. Michaeli. The perception-distortion tradeoff. In *Proceedings of the IEEE Conference on Computer Vision and Pattern Recognition*, pages 6228–6237, 2018.
- [8] T. Boutell. Png (portable network graphics) specification version 1.0. Technical report, 1997.
- [9] M.-M. Cheng, N. J. Mitra, X. Huang, P. H. Torr, and S.-M. Hu. Global contrast based salient region detection. *IEEE Transactions on Pattern Analysis and Machine Intelligence*, 2014.
- [10] D. Dwibedi, I. Misra, and M. Hebert. Cut, paste and learn: Surprisingly easy synthesis for instance detection. In *Proceedings of the IEEE International Conference on Computer Vision*, 2017.
- [11] Forbes. How much data do we create every day? the mind-blowing stats everyone should read, 2018.
- [12] R. Franzen. Kodak lossless true color image suite. *source: http://r0k.us/graphics/kodak*, 4, 1999.
- [13] I. Goodfellow, J. Pouget-Abadie, M. Mirza, B. Xu, D. Warde-Farley, S. Ozair, A. Courville, and Y. Bengio. Generative adversarial nets. In *Advances in neural information processing systems*, pages 2672–2680, 2014.
- [14] K. He, G. Gkioxari, P. Dollár, and R. Girshick. Mask r-cnn. In *Proceedings of the IEEE international conference on computer vision*, 2017.
- [15] K. He, X. Zhang, S. Ren, and J. Sun. Deep residual learning for image recognition. In *Proc. Conf. Comput. Vision Pattern Recognition*, pages 770–778, 2016.
- [16] Q. Hou, M.-M. Cheng, X. Hu, A. Borji, Z. Tu, and P. H. Torr. Deeply supervised salient object detection with short connections. In *Proceedings of the IEEE Conference on Computer Vision and Pattern Recognition*, 2017.
- [17] J. Jiang. Image compression with neural networks—a survey. *Signal processing: image Communication*, 1999.
- [18] D. P. Kingma and J. Ba. Adam: A method for stochastic optimization. *arXiv preprint arXiv:1412.6980*, 2014.
- [19] D. P. Kingma and M. Welling. Auto-encoding variational bayes. *arXiv preprint arXiv:1312.6114*, 2013.
- [20] A. Kolesnikov and C. H. Lampert. Pixelcnn models with auxiliary variables for natural image modeling. In *Proceedings of the 34th International Conference on Machine Learning-Volume 70*, 2017.
- [21] A. Krizhevsky, I. Sutskever, and G. E. Hinton. Imagenet classification with deep convolutional neural networks. In *Neural Inform. Process. Syst.*, pages 1097–1105, 2012.
- [22] J. Lee, S. Cho, and S.-K. Beack. Context-adaptive entropy model for end-to-end optimized image compression. *ICLR*, 2019.
- [23] T.-Y. Lin, M. Maire, S. Belongie, J. Hays, P. Perona, D. Ramanan, P. Dollár, and C. L. Zitnick. Microsoft coco: Common objects in context. In *European conference on computer vision*, 2014.
- [24] S. Luttrell. Image compression using a neural network. In *Proc. IGARSS*, 1988.
- [25] D. Marpe, H. Schwarz, and T. Wiegand. Context-based adaptive binary arithmetic coding in the h. 264/avc video compression standard. *IEEE Transactions on circuits and systems for video technology*, 2003.
- [26] F. Mentzer, E. Agustsson, M. Tschannen, R. Timofte, and L. Van Gool. Conditional probability models for deep image compression. In *Proceedings of the IEEE Conference on Computer Vision and Pattern Recognition*, pages 4394–4402, 2018.
- [27] D. Minnen, J. Ballé, and G. D. Toderici. Joint autoregressive and hierarchical priors for learned image compression. In *Advances in Neural Information Processing Systems*, 2018.
- [28] P. Munro and D. Zipsper. Image compression by back propagation: an example of extensional programming. *Models of cognition: rev. of cognitive science*, 1989.
- [29] Y. Patel, S. Appalaraju, and R. Manmatha. Deep perceptual compression. *arXiv preprint arXiv:1907.08310*, 2019.
- [30] Y. Patel, S. Appalaraju, and R. Manmatha. Human perceptual evaluations for image compression. *arXiv preprint arXiv:1908.04187*, 2019.
- [31] S. Ren, K. He, R. Girshick, and J. Sun. Faster R-CNN: Towards real-time object detection with region proposal networks. *Trans. Pattern Anal. Mach. Intell.*, 39(6):1137–1149, June 2017.
- [32] O. Rippel and L. Bourdev. Real-time adaptive image compression. *arXiv preprint arXiv:1705.05823*, 2017.
- [33] D. E. Rumelhart, G. E. Hinton, and R. J. Williams. Learning representations by back-propagating errors. *Nature*, 323(6088):533, 1986.

- [34] O. Russakovsky, J. Deng, H. Su, J. Krause, S. Satheesh, S. Ma, Z. Huang, A. Karpathy, A. Khosla, M. Bernstein, et al. Imagenet large scale visual recognition challenge. *International journal of computer vision*, 2015.
- [35] C. E. Shannon. A mathematical theory of communication. *Bell system technical journal*, 27(3):379–423, 1948.
- [36] K. Simonyan and A. Zisserman. Very deep convolutional networks for large-scale image recognition. *arXiv preprint arXiv:1409.1556*, 2014.
- [37] A. Skodras, C. Christopoulos, and T. Ebrahimi. The jpeg 2000 still image compression standard. *IEEE Signal processing magazine*, 2001.
- [38] L. Theis and M. Bethge. Generative image modeling using spatial lstms. In *Advances in Neural Information Processing Systems*, pages 1927–1935, 2015.
- [39] L. Theis, W. Shi, A. Cunningham, and F. Huszár. Lossy image compression with compressive autoencoders. *arXiv preprint arXiv:1703.00395*, 2017.
- [40] A. Van den Oord, N. Kalchbrenner, L. Espeholt, O. Vinyals, A. Graves, et al. Conditional image generation with pixelcnn decoders. In *Advances in neural information processing systems*, pages 4790–4798, 2016.
- [41] G. K. Wallace. The jpeg still picture compression standard. *IEEE transactions on consumer electronics*, 1992.
- [42] X. Wang, R. Girshick, A. Gupta, and K. He. Non-local neural networks. In *Proceedings of the IEEE Conference on Computer Vision and Pattern Recognition*, 2018.
- [43] Z. Wang, E. P. Simoncelli, and A. C. Bovik. Multiscale structural similarity for image quality assessment. In *The Thrity-Seventh Asilomar Conference on Signals, Systems & Computers, 2003*, volume 2, pages 1398–1402. Ieee, 2003.
- [44] R. Zhang, P. Isola, E. Efros A.A., Schectman, and W. O. The unreasonable effectiveness of deep features as a perceptual metric. In *CVPR*, 2018.